Modelling and Simulation in
Materials Science and Engineering

Strengthening of edge prism dislocations in Mg–Zn by cross-core diffusion

OPEN ACCESS
IOP Publishing
Modelling and Simulation in Materials Science and Engineering
Modelling Simul. Mater. Sci. Eng. **32** (2024) 065007 (19pp) https://doi.org/10.1088/1361-651X/ad53eb

Strengthening of edge prism dislocations in Mg–Zn by cross-core diffusion

M Rahbar Niazi[1,2,*] **and W A Curtin**[1,2,3]

[1] Laboratory for Multiscale Mechanics Modeling, Institute of Mechanical Engineering, École Polytechnique Fédérale de Lausanne, Lausanne CH-1015, Switzerland
[2] National Centre for Computational Design and Discovery of Novel Materials MARVEL, École Polytechnique Fédérale de Lausanne, Lausanne, Switzerland
[3] School of Engineering, Brown University, Providence, RI 02912, United States of America

E-mail: Masoud.rahbarniazi@epfl.ch

Received 22 November 2023; revised 2 May 2024
Accepted for publication 4 June 2024
Published 20 June 2024

Abstract

The activation of prismatic slip in Mg and its alloys can be beneficial for deformation and forming. Experiments show that addition of Zn and Al solutes have a softening effect at/below room temperature, attributed to solutes facilitating basal-prism-basal cross-slip of prismatic screw dislocations, but a strengthening effect with increasing temperature. Here, the dynamic strain aging mechanism of cross-core diffusion within the prismatic edge dislocation is investigated as a possible mechanism for the strengthening at higher temperatures. First-principles calculations provide the required information on solute/dislocation interaction energies and vacancy-mediated solute migration barriers for Zn solutes around the dislocation core. Results for Mg–0.0045Zn show that cross-core diffusion notably increases the stress for prismatic edge dislocation glide but that the strengthening remains roughly 30% of the experimental strength. Other possible strengthening mechanisms of (i) solute drag of the prism edge dislocation and (ii) solute interactions and/or diffusion within

* Author to whom any correspondence should be addressed.

the prismatic screw core, are then briefly discussed with some quantitative assessments pointing toward areas for future study.

Keywords: cross-core diffusion, prismatic slip, Mg–Zn, first principles, edge strengthening

1. Introduction

The use of lightweight Mg alloys in automotive and aerospace industries could lead to significant reductions in weight, superior energy efficiency and therefore lower emissions. Despite the desirable characteristics of Mg alloys such as high strength-to-weight ratio, high damping capacity, and excellent fatigue resistance, the poor formability of Mg at room temperature has significantly restricted the range of applications of wrought alloys. The poor formability is connected to the anisotropic flow behavior of Mg alloys, which arises from the disparate slip systems in the hexagonally-close-packed (hcp) crystal structure. hcp Mg has two independent a type slip systems on the basal (0001) plane with a very low critical resolved shear stress (CRSS) of $\sim$0.5 MPa. The von-Mises criterion for homogeneous plasticity requires at least five independent slip systems, and so non-basal slip systems or twinning must be activated. However, the CRSS of non-basal prismatic $\left(10\bar{1}0\right)\left[11\bar{2}0\right]$, pyramidal I $\left(10\bar{1}1\right)\left[11\bar{2}3\right]$ and pyramidal II $\left(11\bar{2}2\right)\left[11\bar{2}3\right]$ slip systems are approximately 100 times higher than that of basal slip, and the pyramidal dislocations are also susceptible to a thermodynamically-favorable transformation to a near-sessile structure [1–3]. Reducing the plastic anisotropy by alloying is thus a general goal in the development of Mg alloys.

The activation of prism dislocations is quite useful for sheet forming processes in Mg alloys such as rolling and deep drawing. Prismatic slip provides two additional $\langle a \rangle$ independent slip systems, and so its activation can enhance ductility in plane-strain deformation. Experimental studies [4–6] have shown that prismatic slip above about 150 K is thermally-activated, with the CRSS decreasing rapidly with increasing temperature. At and below room temperature, the addition of dilute solute such as Zn, Al, and Li leads to softening of prismatic slip. For instance, the addition of 0.45% Zn reduces the CRSS by almost 50% at $T = 200$ K and 20% at $T = 250$ K. However, around room temperature, the softening effects disappear and the trend shifts towards strengthening with increasing temperature, although experiments do not show a consistent trend versus solute concentration. Because the prism screw dislocation is unstable versus the basal screw dislocation, prismatic glide is believed to be due to double-cross-slip of basal screw dislocations via thermally-activated nucleation of double kinks [4, 5] or single kinks [7] along the basal screw dislocation. Solute softening at low temperatures and solute strengthening at high temperatures could then be related to a shift deformation from kink nucleation to lateral kink glide, as found in dilute body-centered-cubic (bcc) alloys controlled by screw double-kink nucleation and glide [8]. However, the mechanism for strengthening of prismatic slip at high temperatures is not yet understood. Gaining any fundamental insights into the relevant processes may enable more-informed design of alloys with tailored prismatic slip (as well as solute effects on basal [9, 10] and pyramidal slip [1, 2, 11–15]).

We have recently examined the solute strengthening of prismatic edge dislocations using established quantitative models that have been successfully applied to Al alloys, Mg basal slip, and various high-entropy alloys [16]. First-principles calculations revealed very large solute/dislocation interaction energies for Zn in the prism edge core. But solute-strengthening at dilute Zn concentrations (0.5% or less) remains much smaller than the experimental CRSS

for prism slip in Mg–Zn at all temperatures. The substantial difference in the interaction energies between Zn sites in the core of the dislocation just above and just below the slip plane ($\sim$0.6 eV, see below) provides, however, a very strong driving force for the 'cross-core' diffusion of Zn atoms from the tension side to the compression side of the dislocation core. If there is sufficient Zn and a sufficient diffusion rate, this process can lead to additional strengthening that increases with increasing temperature (due to the increase in diffusion). So, this is a possible mechanism for the observed higher-T strengthening in dilute Mg–Zn alloys. The present paper develops the theory of cross-core diffusion for the Mg prism edge dislocation, presents relevant first-principles results for vacancy-mediated Zn diffusion in the edge core, and quantitatively determines the cross-core strengthening in Mg–0.5%Zn. Results show that the strengthening is significant, compared to the very low strength when no solute diffusion is considered, but that the strength remains 30% of the experimental value. Thus, while cross-core diffusion can be expected, it does not directly control the CRSS of prismatic slip at elevated temperatures and other mechanisms must be investigated.

The remainder of the present paper is organized as follows. In section 2, the theory of solute strengthening is briefly reviewed to provide a basis for strengthening by cross-core diffusion. In section 3, the mechanism, energetics, and kinetics of the cross-core diffusion process are analyzed. The strengthening due to cross-core diffusion in Mg–Zn is calculated and compared with the experimental results in section 4. We summarize our results and examine several additional possible strengthening mechanisms in section 5.

2. Solute strengthening theory

We briefly describe the basic concepts and quantities in the solute strengthening theory of Leyson *et al* [17] and its further developments [18–20]. In dilute alloys, solutes are randomly dispersed within the matrix. As a dislocation glides, segments of the dislocation line pass through a fluctuating energy landscape due to the fluctuations in the local solute positions. A key quantity is the solute/dislocation interaction energy $U(x_i, y_j)$ for an individual solute located at position (x_i, y_j) relative to a dislocation line along z. Figure 1(a) shows the Zn solute/dislocation interaction energies for different sites near the core of the prism $\langle a \rangle$ edge dislocation in Mg as computed using density functional theory near the core (highlighted) and elsewhere using the elasticity approximation $-p(x_i, y_j)\Delta V$ where $p(x_i, y_j)$ is the pressure field created by the edge dislocation and ΔV is the Zn solute misfit volume in Mg. As in [16], the DFT is implemented in VASP [21] with the GGA approximation, the PBE exchange correlation functional [22], PAW pseudopotentials [23] (PAW_PBE Mg 13Apr2007), plane wave energy cutoff of 400 eV, second-order Methfessel–Paxton smearing [24] with parameter 0.2 eV, and Γ-centered Monkhorst–Pack [25] k-mesh with a spacing of 0.01 Å^{-1}. We use a 383-atom simulation cell containing a relaxed edge dislocation at the center shown in figure 1(b).

The statistical fluctuations (i.e. which sites (x_i, y_j) are actually occupied by solutes when the dislocation is at some particular position) lead to collective solute/dislocation interaction energy fluctuations. As discussed in the literature [19], the dislocation thus adopts a wavy configuration so that segments along the line reside in local minimum-energy regions. Minimization of the total dislocation energy (solute potential energies plus elastic line tension) leads to a characteristic segment length ξ_c, a characteristic waviness amplitude w_c, and a characteristic energy barrier ΔE_b at distance w_c that these segments must surmount by thermal activation and applied stress. The local energy landscape for glide of a dislocation segment of length ξ_c can be approximated as $E(x) = \frac{1}{2}\Delta E_b[1 - \cos(\frac{\pi x}{w_c})]$. An applied resolved shear

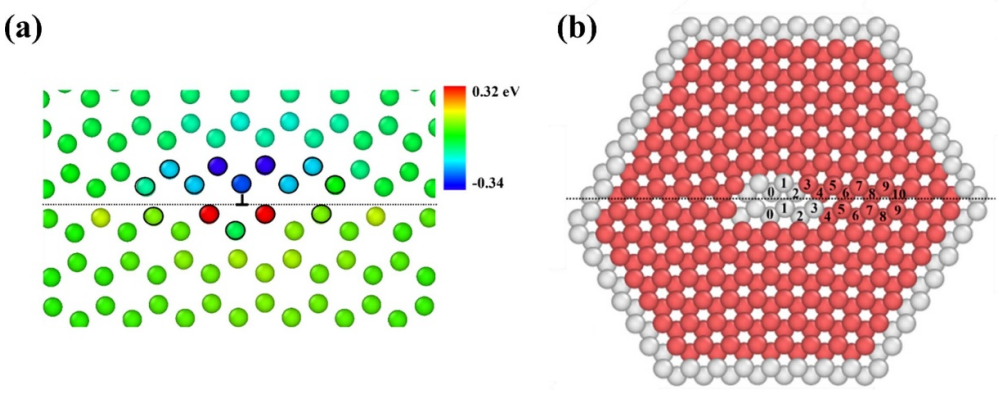

Figure 1. (a) Interaction energies of Zn with the prism edge dislocation. Interaction energies of the sites outlined with black circles are calculated by DFT and the remaining sites computing using the elastic approximation $-p\Delta V$; the dotted line represents the glide plane. (b) DFT supercell (vacuum region of width 10 Å not shown) containing the relaxed edge dislocation without any Zn solute; atoms are colored using common neighbor analysis to differentiate the core region (gray) and boundary region (gray) from hcp atoms (red). Integer labels identify specific sites above/below the slip plane and are used in subsequent analyses.

stress τ does work on the dislocation of Burgers vector b, leading to a total energy landscape $E_{\text{tot}}(x,\tau) = \frac{1}{2}\Delta E_b[1-\cos(\frac{\pi x}{w_c})] - \tau b\xi_c x$. The energy barrier for motion can then be estimated as

$$\Delta E(\tau) = \Delta E_b \left(1 - \frac{\tau}{\tau_{y0}}\right)^{\frac{3}{2}} \tag{1}$$

where τ_{y0} is the zero-temperature yield stress at which the barrier is reduced to zero and glide occurs with no thermal activation. Glide at temperature T occurs at a rate R by thermal activation according to an Arrhenius law

$$R = \nu_0 \exp\left(-\frac{\Delta E(\tau)}{k_{\text{B}}T}\right) \tag{2}$$

where ν_0 is an attempt frequency and k_{B} is Boltzmann's constant. Each segment advances by $2w_c$ and so the macroscopic strain rate $\dot{\varepsilon}$ due to the motions of the mobile dislocation density ρ_m is, via Orowan's law,

$$\dot{\varepsilon} = \dot{\varepsilon}_0 \exp\left(-\Delta E(\tau)/k_{\text{B}}T\right) \tag{3}$$

where $\dot{\varepsilon}_0 = 2\rho_m b w_c \nu_0$ is a reference strain rate. Inverting this relationship leads to the yield stress τ_y as a function of T and $\dot{\varepsilon}$ as

$$\tau_y(T,\dot{\varepsilon}) = \tau_{y0}\left[1 - \left(\frac{k_{\text{B}}T}{\Delta E_b}\ln\frac{\dot{\varepsilon}_0}{\dot{\varepsilon}}\right)^{\frac{2}{3}}\right]. \tag{4}$$

The application of this solute strengthening theory to Mg–0.0045Zn, using the Zn/prism edge interaction energies in figure 1, has been discussed fully in [16]. The energy barrier and zero-T strength are, respectively, $\Delta E_b = 0.51$ eV and $\tau_{y0} = 21.4$ MPa while the characteristic lengths are $\zeta_c = 147$Å and $w_c = 4b = 12.76$ Å.

When kinetic processes occur, an important quantity is the average waiting time t_w of the dislocation segments. This is the average time that a segment sits in its local solute environment before it is thermally-activated to the next local minimum environment. From Orowan's law, the waiting time at strain rate $\dot{\varepsilon}$ is

$$t_w = \frac{2\rho_m b w_c}{\dot{\varepsilon}}. \tag{5}$$

3. Cross-core diffusion in Mg–Zn

3.1. Mechanism

Since solutes interact with the dislocation (see figure 1), solutes prefer to reside at atomic sites with the largest negative interaction energies. There is thus a thermodynamic driving force for solutes to move from higher (less negative) energy sites to lower (more negative) energy sites. Any such motion requires vacancy-assisted diffusion, which depends on the vacancy concentration, solute migration barriers, and temperature. At low temperatures, the vacancy concentration is low and the solute migration rate is very slow so that diffusion is unable to occur during the waiting time. With increasing temperature, diffusion can occur faster, and solutes will migrate to the lower-energy sites around the dislocation. Due to the strong driving force across the core and due to reduced migration barriers in the core (see below), the dominant diffusion is 'cross-core' [26] from sites on the tension side just below the glide plane to adjacent sites on the compression side (for Zn solutes in Mg). Solute diffusion from sites further from the core tends to be much slower due to the negligible driving forces and higher migration barriers [26]. Figure 2, derived from figure 1, shows the dominant cross-core diffusion paths in Mg–Zn and the associated energetic driving forces; sites are labeled by an integer and 'top' or 'bottom' relative to the glide plane. We will justify the choice of these subsets of diffusion paths later by analysis of the migration barriers.

As solutes diffuse to energetically-favorable sites, the energy of the system with the dislocation in its current position is lowered. That is, the dislocation becomes increasingly pinned at its current location. There is then a larger energy barrier for dislocation motion and hence a higher stress must be applied to sustain an imposed strain rate. Since diffusion increases with increasing temperature, the alloy can be strengthened with increasing temperature. Cross-core diffusion is thus a mechanism of dynamic strain aging (DSA), and was introduced and analyzed in the context of long-standing DSA effects in fcc Al-Mg alloys [27].

Given the driving forces for cross-core diffusion of Zn in Mg, the determination of the strengthening as a function of temperature at a specified strain rate requires several steps of analysis. First, the energy change of the system (dislocation plus solutes) due to diffusion must be established. Second, the change in the stress-dependent energy barrier for dislocation motion must be determined. Third, the solute diffusion kinetics between the various sites in and around the core must be computed. Assembling these components, the net effects of cross-core diffusion on strengthening can be determined as a function of temperature and solute concentration. These steps are described in detail in the following sections.

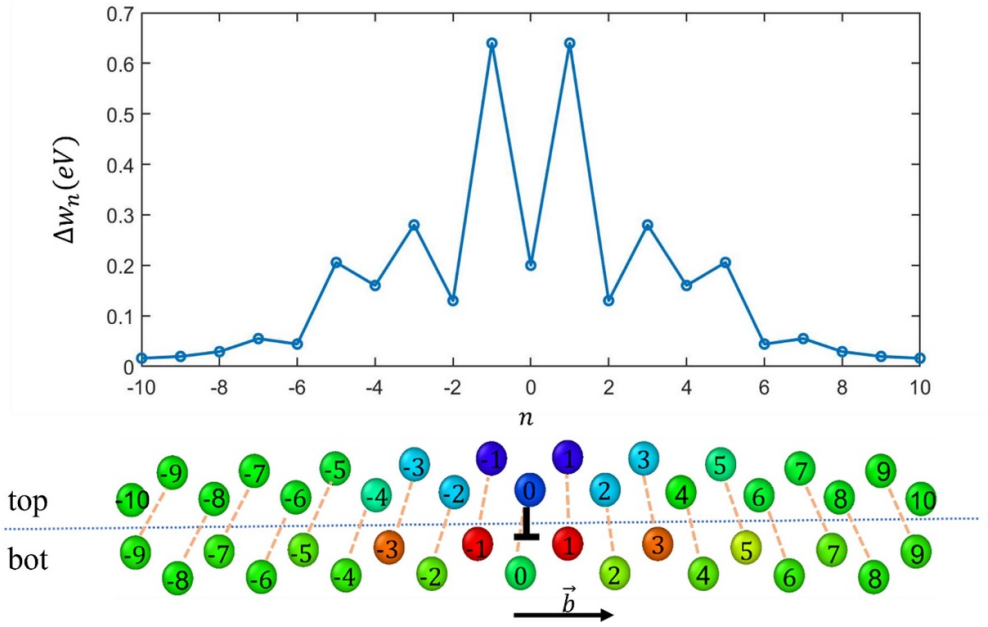

Figure 2. The difference in the Zn/dislocation interaction energy Δw_n between the sites n below and above the glide plane and connected by dashed lines. Atoms are labeled by the integer n according to their lateral position away from the center of the dislocation core.

3.2. *Energetics*

Starting from figure 1, we label sites as n^{bot} and n^{top}, as shown in figure 2, according to whether they are above or below the glide plane, and numbered versus lateral (glide) distance from the center of the core. The solute/dislocation interaction energy for a Zn atom at each site is then labeled as w_n^{top} or w_n^{bot}.

Before any cross-core diffusion, at time $t = 0$, the energy of the system contained in an average random solute environment at solute concentration c_0 is

$$E(t=0) = \sum_n c_0 \left(w_n^{\text{top}} + w_n^{\text{bot}}\right). \tag{6}$$

While dislocations actually reside in locally-favorable solute configurations, it is not feasible to consider the cross-core diffusion starting from individual local configurations. The cross-core contribution to strengthening is also fairly independent of the initial state because the solute strengthening depends on many solutes around the core (see [28])—not just those in the core—and the local fluctuations of the few solutes just above and below the core is not a dominant contributor to the overall strengthening.

After a time t during which solute diffusion has occurred, the solute concentrations in each site will change from c_0 to $c_n^{\text{top}}(t)$ and $c_n^{\text{bot}}(t)$. The energy of the system after cross-core diffusion for time t is then

$$E(t) = \sum_n \left[c_n^{\text{top}}(t)\, w_n^{\text{top}} + c_n^{\text{bot}}(t)\, w_n^{\text{bot}}\right]. \tag{7}$$

The concentration evolution $\left(c_n^{\text{top}}(t), c_n^{\text{bot}}(t)\right)$ of different sites will be considered in the next section.

The energy landscape that determines dislocation glide is then determined, in the presence of the cross-core diffusion, by considering motion of the dislocation in increments of one Burgers vector while the solutes remain fixed in their positions. The position of the dislocation relative to the solutes is thus changing or, conversely, the position of the solutes relative to the dislocation is changing (in the opposite direction). Glide of the dislocation by one Burgers vector shifts a solute at original site n to a new relative position $n-2$ with respect to the dislocation core. The concentration of this site remains unchanged, but its interaction energy with the dislocation has changed by virtue of its new position relative to the dislocation. Therefore, after dislocation glide over a distance $x = mb$, the energy of the dislocation is

$$E(t, x = mb) = \sum_n \left[c_n^{\text{top}}(t)\, w_{n-2m}^{\text{top}} + c_n^{\text{bot}}(t)\, w_{n-2m}^{\text{bot}}\right]. \tag{8}$$

After some algebra, we obtain the change in energy at time t and dislocation glide $x = mb$, relative to the initial energy at time $t = 0$, as

$$\Delta E_{xc}(t, x = mb) = E(t, x = mb) - E(0,0) = \sum_n \left[\Delta c_n^{\text{top}}(t)\, w_{n-2m}^{\text{top}} + \Delta c_n^{\text{bot}}(t)\, w_{n-2m}^{\text{bot}}\right] \tag{9}$$

where $\Delta c_n^{\text{top/bot}} = c_n^{\text{top/bot}} - c_0$. Since the driving force decays with distance from the core (increasing n), the energy change is the largest (most negative) at the initial position $m = 0$. The energy change slowly increases with increasing glide distance mb until it reaches zero. At this point, there are no longer any diffused solutes inside the current position of the core—all diffused solutes have been left far behind the core and have (nearly) zero interaction energy with the core in its present position.

The energy change of equation (9) creates the additional barrier for dislocation motion due to cross-core diffusion. The total energy barrier is then the sum of the pre-existing random solute energy landscape with barrier ΔE_b and the additional cross-core energy barrier ΔE_{xc} With application of an external stress τ, the total energy of the dislocation segment at time t and position $x = mb$ is

$$E(t, x = mb, \tau) = \frac{1}{2}\Delta E_b \left[1 - \cos\left(\frac{\pi x}{w_c}\right)\right] + \left(\frac{\xi_c}{1.62b}\right) \Delta E_{xc}(t, x = mb) - \tau b \xi_c x \tag{10}$$

where 1.62 is the c/a ratio of the hcp lattice. Equation (10) is the basis for determining the stress-dependent and time-dependent energy barrier. We will apply equation (10) at the waiting time $t = t_w$ which, while not exact (see [27, 29]), enables efficient evaluation of the strengthening. To determine the quantitative strengthening then requires the determination of the solute concentrations $c_n^{\text{top}}(t), c_n^{\text{bot}}(t)$ as a function of time t and site n, which is discussed in the next section.

3.3. Kinetics

Due to the variations in solute/dislocation interaction energy versus specific position along the dislocation core, an analysis requires consideration of all individual solute diffusion paths. Figure 3 shows a close-up schematic of the cross-core diffusion paths considered in this study, indicated by dashed lines and where, due to symmetry, only sites to the right of the dislocation

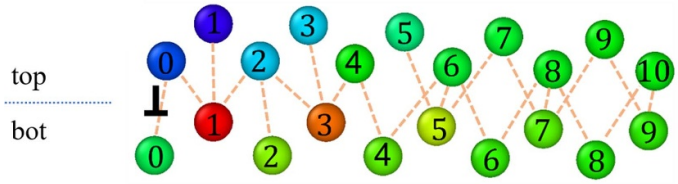

Figure 3. Potential cross-core diffusion paths considered in this study.

core ($n \geqslant 0$) are shown. This schematic is a projected view of the atomistic core along the dislocation line, and all the paths shown are between sites that can be considered as neighbors based on interatomic distance. The high distortions in the core lead to differences between 'core' and 'bulk' site coordination; for instance, sites 7^{bot} and 9^{top} away from the core are near neighbors in the hcp crystal structure but the seemingly-corresponding sites 1^{bot} and 3^{top} in the core are too far apart to be considered as neighbors. We consider only cross-core diffusion. Diffusion could occur in principle between neighboring sites on the same side of the slip plane but the driving forces are much smaller and the migration barriers are much closer to the (larger) bulk migration barrier; as briefly discussed in section 5, including lateral paths has a negligible effect on strengthening.

For a given set of allowed diffusion paths, we use a discrete form of the master equation for the evolution of the concentrations of all sites [30]. In general, for a set of sites $\{i\}$, the master equation is a coupled system of partial differential equations describing the concentration evolution $c_i(t)$ of each site i accounting for the flux of solutes flowing into site i from neighbors $\{j\}$ with activation barriers $Q_{j\to i}$ and out of site i into sites $\{j\}$ with activation barriers $Q_{i\to j}$. Specifically, the rate of change of $c_i(t)$ is

$$\frac{\partial c_i}{\partial t} = \sum_{j=1}^{z} \left[c_j (1-c_i)\, \nu_0 \exp\left(-\frac{Q_{j\to i}}{k_{\text{B}}T}\right) - c_i (1-c_j)\, \nu_0 \exp\left(-\frac{Q_{i\to j}}{k_{\text{B}}T}\right) \right] \quad (11)$$

where z is the number of neighbors of site i. The activation energy for diffusion is the sum of the vacancy formation energy ΔH_{vf} and the migration barriers $E_{\text{mig}}^{j\to i}$ and $E_{\text{mig}}^{i\to j}$,

$$\begin{aligned} Q_{j\to i} &= \Delta H_{\text{vf}} + E_{\text{mig}}^{j\to i} \\ Q_{i\to j} &= \Delta H_{\text{vf}} + E_{\text{mig}}^{i\to j} \end{aligned} \quad . \quad (12)$$

In this formulation, the vacancies necessary to accomplish the solute motion are implicit. We apply this formulation to all the pairs of sites where cross-core diffusion is considered, as indicated in figure 3.

Since vacancies also interact rather strongly with the dislocation core, the general formulation above must be adapted to consider the overall diffusion process. Such details were neglected in the original cross-core diffusion work, in part because the vacancy/dislocation interactions in Al were much smaller than we find here (see below) for the compact edge prism core in Mg. In principle, the dislocation arrives at its current location at $t = 0$ and the vacancies in the vicinity are randomly distributed with equal probability at every atomic site independent of the dislocation. Diffusion normally assumes that the probability of a vacancy at the necessary site for solute diffusion is equal to the bulk vacancy concentration; this is why the vacancy formation energy appears in the master equation. However, there are very few vacancies, and so the actual underlying assumption is that the vacancy diffusion itself is fast enough to enable

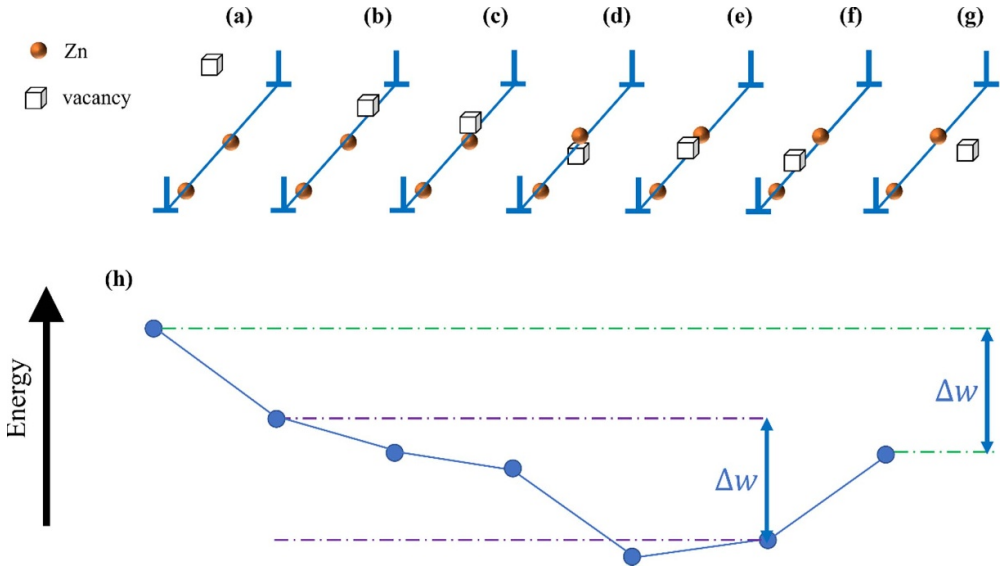

Figure 4. (a)–(g) Schematic representation of the sequence of atomistic configurations relevant to the cross-core diffusion process involving a vacancy, a solute, and a dislocation, (h) schematic of the corresponding energies, with the net driving force Δw shown as the difference between configurations (b), (f) or (a), (g).

vacancies to arrive adjacent to the solute so that it is suitable to use the equilibrium vacancy concentration as the probability that a vacancy is present.

In actuality, the situation is better represented by the schematic in figure 4 showing the overall process by which Zn solutes diffuse across the core. At $t = 0$ when the dislocation arrives at its current position, there are Zn atoms along the core and vacancies somewhere around the core (figure 4(a)). In the first stage, a nearby vacancy will diffuse to the core, aided in part by the attractive elastic vacancy/dislocation interactions (figure 4(b)). The vacancy migration energy in bulk Mg is 0.40 eV, and so there is significant diffusion of existing vacancies at the temperatures of interest (e.g. at 400 K the vacancy can make $\sim 2 \times 10^6$ random transitions in the bulk during the waiting time). The vacancy/dislocation interactions in the core are large, with DFT computations showing vacancy binding energies of -0.44 eV and -0.39 eV at sites 0^{top} and 1^{top}, respectively. A vacancy reaching the core will thus remain in the core, diffusing in/around the core region, and eventually arrive at a site adjacent to a Zn atom on the other side of the core (figure 4(c)). The 'cross-core' diffusive step corresponding to exchange of the vacancy and Zn can then occur (figure 4(d)). However, the vacancy formation energy for sites on the other side of the core is more positive (e.g. -0.26 eV at site 0^{bot} and $+0.02$ eV at site 1^{bot}) and so the energy lowering due to the Zn binding (see figure 2) is partially offset by the increase in energy due to the vacancy binding. The vacancy can then, however, diffuse to another neighboring site on the favorable (lower energy) side of the core, with a significant reduction in the system energy (figure 4(e)). The vacancy can then move away from the Zn atom (figure 4(f)), diffusing to other locations and facilitating further cross-core diffusion events. Binding of the vacancy/Zn pair can inhibit this last process, but this is offset by the entropy gained in enabling the vacancy to explore more sites in the core. In principle, the vacancy can also move back into the bulk Mg (away from the core) as in figure 4(g), but this is much less favorable due to the strong vacancy binding in the core. The net result of these diffusion processes is the

'cross-core diffusion' of the Zn atom with an energy gain $\Delta w = w^{\text{top}} - w^{\text{bot}}$, independent of the vacancy energetics and diffusion. Figure 4(h) shows a schematic of the relative energies of each configuration in figures 4(a)–(g). The net cross-core driving force Δw is indicated and can be associated with the energy difference between figures 4(d) and (f) or figures 4(a) and (g). The energy difference between figures 4(c) and (e) differs from Δw only by the difference in vacancy-Zn binding energies in the two configurations.

The sequence of configurations in figure 4 illustrates that there are many paths by which an actual vacancy can arrive at a position adjacent to a Zn atom in the core, as the vacancy explores the system. All of the vacancy diffusion steps occurring away from the solute are assuming the existence of an initial vacancy, and are not embedded in the master equation. The assumption in the master equation is thus that there is a vacancy at the necessary site adjacent to the Zn with a probability given by the vacancy concentration $c_v = \exp(-\frac{\Delta H_{\text{vf}}}{k_B T})$, entering through the presence of ΔH_{vf} in the $Q_{i\to j}$ and $Q_{j\to i}$.

The initial and final states for cross-core solute migration are those in which the vacancy is remote from the Zn atom, and so can then be taken as configurations shown in figures 4(b) and (f), respectively, with the energy difference being the driving force Δw. The relevant migration barriers for cross-core diffusion *(b)–(f)* and its reverse process *(f)–(b)* are then determined by the highest energy point along the transition path from *b* to *f that involve the Zn solute,* and hence the highest point along the transition path from *c* to *e*. Due to the large decrease in energy between configurations *d* and *e*, the controlling cross-core barrier is expected to be the step from *c* to *d*, corresponding to the motion of the Zn atom. The reverse barrier from *f* to *b* will differ by Δw and so will automatically satisfy detailed balance (which is embedded in the master equation).

We use the nudge elastic band (NEB) method in DFT to compute the transition paths between configurations *c* and *d* using 5 intermediate images. Niazi and Curtin [16] provides details of the dislocation construction method, size, and energy minimization used. A vacancy and Zn atom are introduced into the relaxed simulation cell, and further ionic relaxations are performed holding all ions within 4 atomic planes of the outer boundaries fixed at the relaxed dislocation-only configuration while periodic boundary conditions are maintained along the dislocation line. Initial and final states for the NEB calculation are obtained by relaxing all other ions until all forces are below 10 meV Å^{-1} and electronic degrees of freedom are converged at 10^{-8} eV.

During the NEB calculation, the minimum energy path (MEP) is found by minimizing the true ionic forces on each image perpendicular to the path and the spring forces between the images along the path in order to keep the images equi-distant. The transition state is the highest energy state along the MEP. The transition state is a saddle point at which both perpendicular and parallel components of the ionic force should vanish. Here, we use the NEB algorithm in VASP but use the two convergence criteria of perpendicular and total ionic force both below 10 meV Å^{-1} in the transition state replica.

NEB calculations were performed for Zn-Vacancy exchange among the pairs of sites shown in figure 5(a) with the corresponding barrier energies indicated. The MEPs for these transitions are shown in figure 5(b). A number of these cross-core paths have very low (<0.1 eV) migration barriers due to a combination of the distorted core environment and the net driving force for the transition. Thus, cross-core diffusion in these paths is very fast relative to bulk diffusion. We note in figure 5(b) that the energy differences between initial and final states (configurations *c* and *d* in figure 4) for paths near the core remains fairly small because of the competition between Zn and vacancy binding energies in the core.

Paths such as $1^{\text{bot}} - 0^{\text{top}}$ and $1^{\text{bot}} - 2^{\text{top}}$ are between sites in different atomic planes with atomic distances of ∼3.6 Å that are much larger than other pairs (e.g. the atomic distance

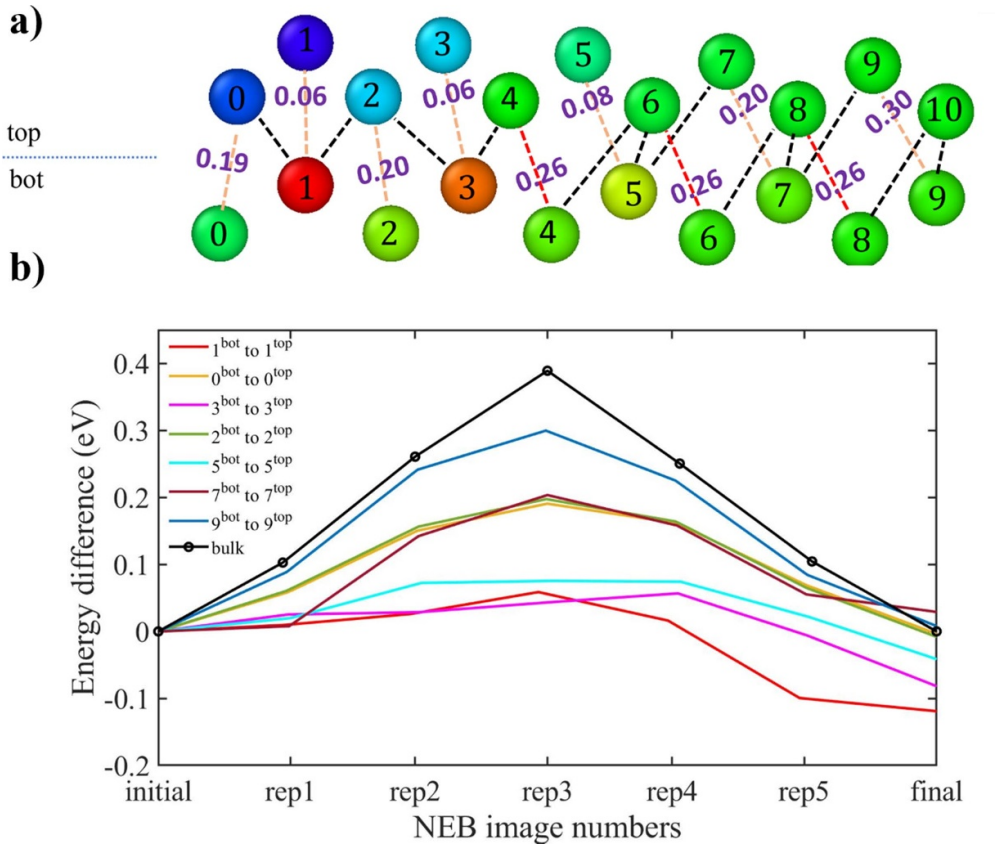

Figure 5. (a) Cross-core diffusion paths considered, with initial 'bottom' states (figure 4(c)) and final 'top' states (figure 4(f)). Orange dashed lines represent the paths with DFT calculated barriers. Dashed red lines represent barriers for paths assumed to be the average value of the barriers along the forward and backward direction of path $2^{bot} - 2^{top}$. The barriers of the paths shown by black dashed lines are assumed to be the bulk barrier, 0.39 eV. (b) Minimum energy path versus NEB image/replica, for the cross-core paths shown by the dashed orange lines in (a) and for bulk migration.

for $1^{bot} - 1^{top}$ is 3.03 Å) so we expect these barriers to be significantly larger than 0.2 eV. For instance, although not shown in figure 5, the path $3^{bot} - 5^{top}$ (with distance 3.9 Å) has an NEB-computed migration barrier of 0.49 eV in spite of the large driving force, and we expect path $1^{bot} - 3^{top}$ to be similar and so diffusion between these pairs is neglected. Then, for those paths shown in figure 5(a) with dashed black lines that also have distances greater than the bulk distance, and paths further from the core (not shown), are assigned the bulk migration barrier $E_{mig}^{bulk} = 0.38$ eV for migration along the basal plane. Paths $4^{bot} - 4^{top}$, $6^{bot} - 6^{top}$, and $8^{bot} - 8^{top}$ (represented by red dashed lines) have distances less than the bulk interatomic distance but are further from the core than $2^{bot} - 2^{top}$ and with negligible driving force so their barriers are most likely higher than 0.2 eV; we use the value 0.26 eV that is the average of the forward and reverse barriers for path $2^{bot} - 2^{top}$. Analysis and testing show that the final results for cross-core strengthening are *not* sensitive to the precise values of these higher-barrier paths. Therefore, due to high computational cost, we did not compute precise values.

Two cases, $3^{\text{bot}}-3^{\text{top}}$ and $9^{\text{bot}}-9^{\text{top}}$, did not reach our convergence criterion for the total ionic force near the transition state, reaching only ∼25 meV Å^{-1} after 60 iterations. However, in both cases, the image near the transition state had perpendicular forces well below 10 meV Å^{-1} indicating that the image is along the MEP. Thus the estimated barrier using this image is a lower bound to the true barrier. Since the barriers in these two cases were 0.06 and 0.30 eV, and the change in total energy with increasing the number of iterations were negligible compared to these values, we did not attempt to converge these transition state images further.

4. Results

In the previous section, we computed the migration barriers for cross-core diffusion, and so we can now calculate the concentration evolutions of $c_n^{\text{top}}(t), c_n^{\text{bot}}(t)$ using the framework of equation (11). Then, using equation (10), we can calculate the energy landscape for dislocation glide versus time. We determine the yield strength using the concentration changes at the waiting time t_w. The details and results are as follows.

For the prism edge dislocation in Mg–0.45%Zn, with a typical dislocation density in a well-annealed crystal of $\rho_m = 10^{12}$ m^{-2} and at typical experimental strain rate $\dot{\varepsilon} = 1.66 \times 10^{-4}$ s^{-1}, the average waiting time of $t_w = 0.0049$ s. Equation (11) is thus solved numerically for 112 sites (112 equations) located to the right and left sides of the dislocation center, on both bottom and top sites along the slip plane for this waiting time. The initial conditions are solute concentration $c_i = 0.0045$ for all sites. Figure 6 shows the concentration profiles $c_n^{\text{top}}(t_w), c_n^{\text{bot}}(t_w)$ for different temperatures. The equilibrium vacancy concentration is also shown for each temperature using $\Delta H_{\text{vf}} = 0.79$ eV. At $T = 300$ K, no cross-core diffusion is observed because the vacancy concentration is too low (the cross-core migration barriers in the core being so low that vacancy concentration dominates the rate). Noticeable diffusion begins at $T = 350$ K where Zn solutes are diffusing from bottom to top sites near the center of the core where the migration barriers are very low (odd numbered pairs of sites). At $T = 400$ K, the concentration of site 1^{top} is twice the initial concentration as a result of complete diffusion of all solutes at site 1^{bot} into site 1^{top}. At $T = 450$ K, the diffusion into nearby top sites (odd numbers) also reaches the maximum values while some diffusion along other paths with higher migration barriers (sites labeled with even numbers) begins. At $T = 500$ K, there is more extensive diffusion, with activation of paths such as $4^{\text{bot}}-4^{\text{top}}$.

Figure 7 shows the total energy landscapes $E(t, x = mb, \tau = 0)$ computed using equation (10) at the waiting time and under zero stress, for different temperatures as derived from the concentration fields shown in figure 6. The total energy consists of the initial solute strengthening contribution plus the additional contribution due to cross-core diffusion contribution $\Delta E_{xc}(t, x = mb)$, which is also shown separately as the red curve. With increasing temperature, the energy at the initial dislocation position $x = 0$ decreases steadily due to the increasing cross-core diffusion. The effect of the cross-core diffusion extends out to dislocation glide distances of $\sim 2w_c$ but the main energy lowering is in the regime $x < 1.5w_c$.

For plastic flow to occur, the stress must be sufficiently large to drive the system to lower total energy when the dislocation has moved to the next local minimum solute environment at typical distance $2w_c$. At any lower stress, if the dislocation glides by thermally-activation over the barrier to the next local minimum, the barrier for the reverse motion, returning the dislocation to the initial state, is smaller and the dislocation will rapidly return to the initial state. The net rate of plastic deformation at temperature T is then the difference between the

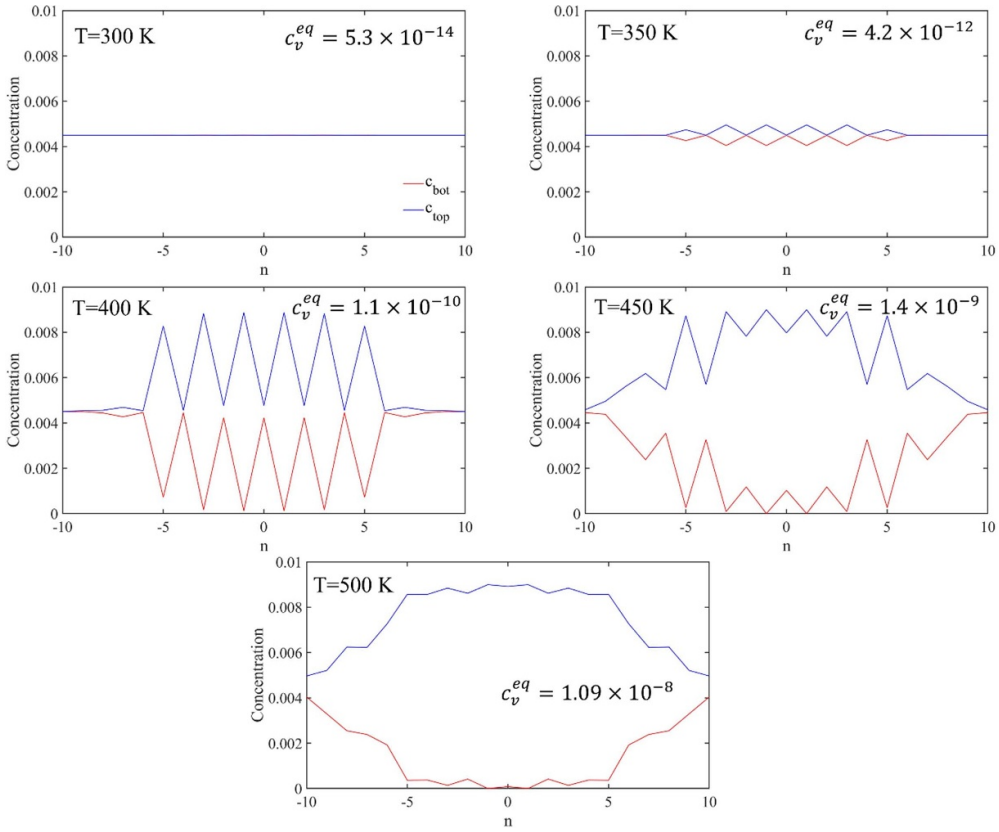

Figure 6. Solute concentration profiles after cross-core diffusion over the dislocation waiting time t_w versus site n in the core (top sites in blue, bottom sites in red), for increasing temperatures as indicated. The equilibrium vacancy concentration at each temperature is also shown.

glide rates in the forward and reverse directions, with energy barriers E_b^f and E_b^r respectively, so that

$$\dot{\varepsilon} = \dot{\varepsilon}_0 \left[\exp\left(-\frac{E_b^f(T,\tau)}{k_B T} \right) - \exp\left(-\frac{E_b^r(T,\tau)}{k_B T} \right) \right]. \tag{13}$$

Using equation (10), the barriers E_b^f and E_b^r, evident in figure 7, are computed as a function of temperature. At the specified strain rate, the shear stress at which equation (13) is satisfied is the yield stress (CRSS). As an example, figure 8 shows the energy landscapes at $T = 450$ K for increasing applied stresses. At the experimental strain rate of $\dot{\varepsilon} = \ 1.66 \times 10^{-4}\ \mathrm{s}^{-1}$, the shear yield stress at $T = 450$ K is 4.4 MPa.

Calculations of the yield stress versus temperature at $\dot{\varepsilon} = \ 1.66 \times 10^{-4}\ \mathrm{s}^{-1}$ are shown in figure 9. At low temperatures, there is no cross-core diffusion, and the strength is due solely to static solute strengthening, and is well below experiments. At $T = 350$ K and above, the cross-core diffusion leads to non-negligible strengthening that shows a saturation of $\tau_y \sim 4.5$ MPa versus temperature up to $T = 500$ K. The cross-core diffusion of Zn solutes at a concentration

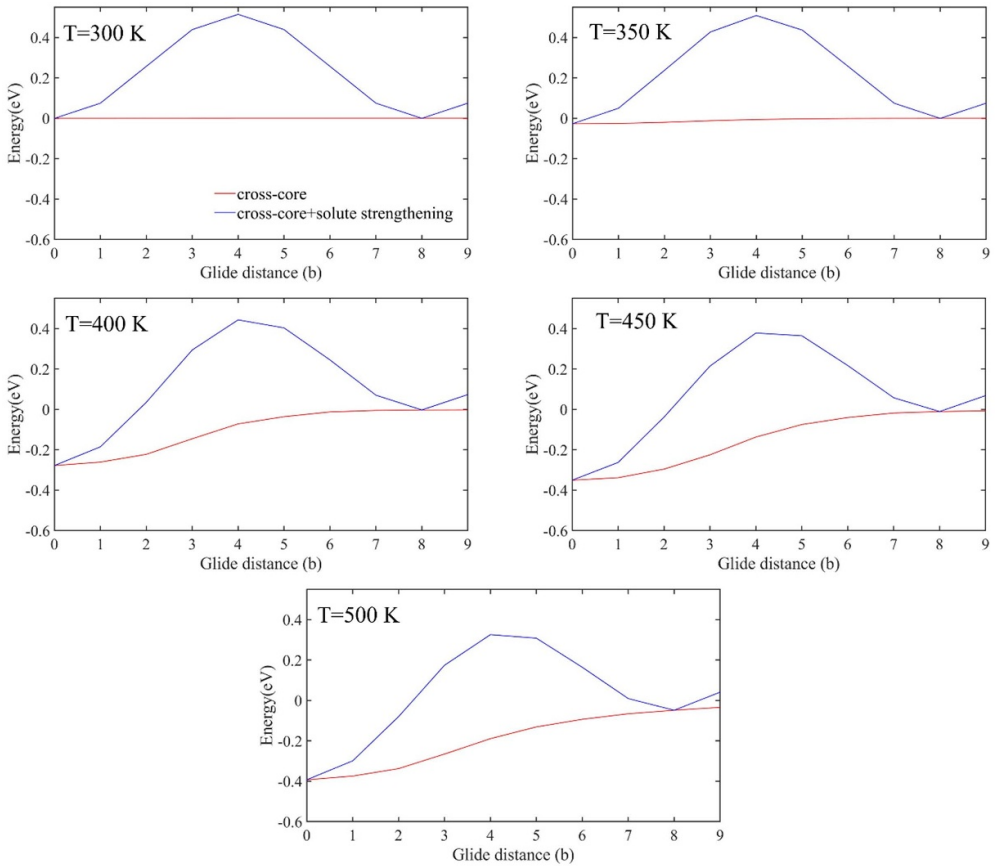

Figure 7. Energy versus dislocation glide distance (in units of b) due to cross-core diffusion at the waiting time t_w and under zero stress, for different temperatures (blue lines); the contribution due to cross-core diffusion alone is shown as the red line.

of 0.0045, while non-negligible, is thus not sufficient to explain the experimentally-measured strength. This is the main conclusion of the present work.

The apparent increasing strength with increasing temperature for 300 K $< T <$ 400 K, which is equivalent to an apparent negative strain rate sensitivity, is an artifact of fixing the dislocation waiting time. Theory (see [29]) shows that the strain rate sensitivity can never be negative due solely to cross-core diffusion of mobile dislocations. Hence, the true behavior will be a plateau in strength at ∼4.5 MPa over an extended temperature range including below $T <$ 400 K. The full calculation is, however, not computationally feasible and, since it does not affect our main conclusion, we have not attempted to execute it.

5. Discussion

We have studied the cross-core diffusion of Zn solutes on the strength of the prism edge dislocation in Mg, motivated by the very large energetic driving force computed by first-principles DFT (figure 2). In addition to a large driving force, the migration barriers for cross-core diffusion of Zn in the core are found to be very small (figure 5), enabling cross-core diffusion to

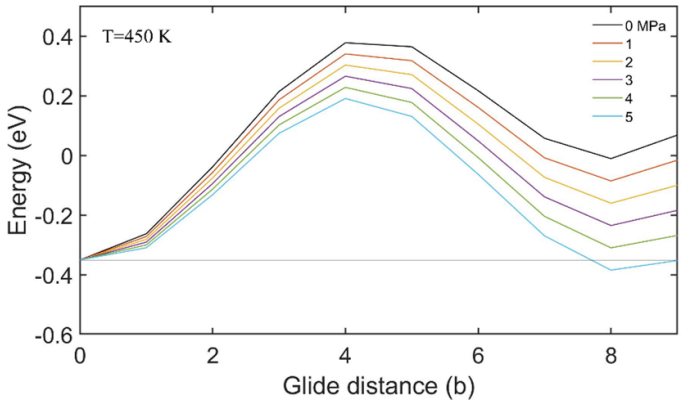

Figure 8. Energy versus glide distance, after cross-core diffusion over the waiting time, for different applied stresses at $\dot{\varepsilon} = \ 1.66 \times 10^{-4}$ s^{-1} and $T = 450$ K. Plastic flow occurs when the net rate of motion matches the strain rate (see equation (13)), requiring >4 MPa under these conditions.

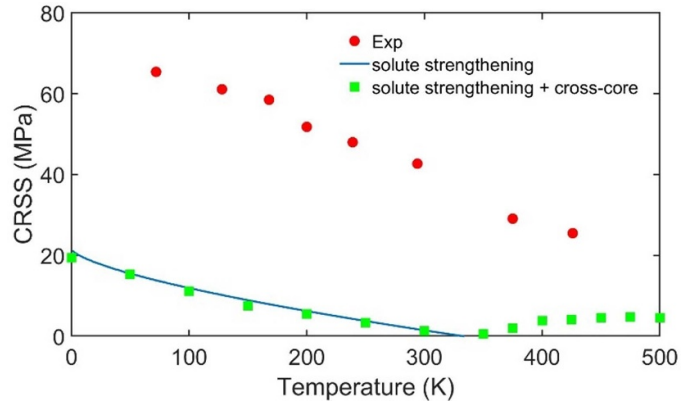

Figure 9. Yield strength versus temperature, as measured (red) and as predicted by solute strengthening plus cross-core diffusion (green). The contribution due to solute strengthening is shown as the blue line.

occur very easily in the presence of a vacancy. However, the vacancy concentration remains very low at $T = 300$ K and below and greatly limits cross-core diffusion during the dislocation waiting time, leading to no strengthening. At temperatures $T = 350$ K and above, the Zn solute diffusion becomes fast enough to create strengthening but the strengthening saturates at ∼4.5 MPa, lower than the experimental strength of ∼25 MPa at $T = 425$ K. Thus, while cross-core diffusion can operate at these temperatures, the Zn concentration of 0.0045 remains too low to create the strengthening observed in experiments.

In this study, we did not consider lateral diffusion between sites located on the same side of the slip plane. These additional diffusion paths could lead to higher solute concentrations at the lowest solute binding sites (0^{top}, 1^{top}), leading to further lowering of the dislocation energy and increasing of the CRSS. However, repeating our analysis by including additional lateral paths $0^{\text{top}} - 1^{\text{top}}$ ($E_{\text{mig}} = 0.22$ eV, $\Delta w = -0.08$ eV) $2^{\text{top}} - 1^{\text{top}}$ ($E_{\text{mig}} = 0.14$ eV, $\Delta w = -0.16$ eV), and $2^{\text{top}} - 0^{\text{top}}$ ($E_{\text{mig}} = 0.22$ eV, $\Delta w = -0.16$ eV) with optimistically low migration barriers

estimated as $E_{\text{mig}} = 0.30 + \Delta w$ increases the strength by only $\sim$2 MPa. Furthermore, these paths would only be activated at $T > 400$ K. It is also possible that the real solute/dislocation interaction energies could be higher than computed by DFT, leading to higher strengths, but repeating our analysis with solute/dislocation interaction energy of sites 0^{top} and 1^{top} by increased by 0.1 eV results in a negligible 0.02 eV increase in the total energy barrier. Finally, the vacancy concentration could be larger if the vacancy formation free energy is lower than the $T = 0$ K value used here. However, this would mainly shift the temperature range of cross-core diffusion to slightly lower temperatures without significant change in the magnitude of the strengthening.

Since strengthening by cross-core diffusion does not reach values comparable to experiments, we here briefly assess other possible strengthening mechanisms. With a low Zn migration barrier, Zn diffusion at higher temperatures might enable the operation of solute drag of the prism edge dislocation. Solute drag is due to the formation of a steady-state solute cloud that trails a steadily-moving dislocation, and is controlled more by the solute cloud outside of the core than by cross-core diffusion. Data on Al–0.0052 Mg [30], with a similar concentration and bulk diffusion activation energy (vacancy formation plus migration of 1.28 eV) as Mg–0.0045Zn, shows strengthening of 5–10 MPa at $T = 600$ K. It is thus valuable to estimate solute drag strengthening in Mg–Zn. We use results of Zhang and Curtin [30], who used the Master equation for discrete diffusion around an FCC edge dislocation core described by a Peierls–Nabarro model with core-spreading parameter of $\zeta = 1.5b$. This value is close to the core spreading of $\zeta = 1.6b$ derived from the Mg prism edge structure shown in figure 1. James and Barnett [31] had previously used a continuum model for the same problem. Zhang and Curtin [30] found the maximum solute drag strengthening to be $\tau_{\text{max}} \cong 0.5c\frac{\mu}{3\pi}\frac{1+\nu}{1-\nu}(\frac{\Delta v}{v_a})$ where Δv and v_a are the solute misfit volume and atomic volume, respectively, in a material with shear modulus μ and Poisson's ratio ν. James and Barnett showed the same scaling but with a pre-factor of 0.25. Using the material values for Mg–0.0045Zn, the maximum solute drag strengthening is estimated as 2.5 MPa. This strength remains well below the experiments. Therefore, *independent of the strain rate at which this maximum strengthening occurs*, the solute drag mechanism is unlikely to be responsible for the observed strengthening of Mg–Zn at high temperatures.

With screw dislocations controlling the stress at low temperatures [4, 5] it is also possible that there is a DSA phenomenon related to Zn diffusion in the screw dislocation core. Normally DSA is not associated with screw dislocations because there is no long-range pressure field to attract solutes. However, solute/screw interactions in the core exist and can drive local segregation. To begin an investigation of this issue, we have performed first-principles calculations of the interaction energy of Zn with the prism screw core; DFT details are the same as those used for the edge core. The prism screw core is unstable in pure Mg [32] and so we stabilize this core by placing a Zn solute at the center of the core (position just below the S in figure 10). We then measure the Zn/screw interaction at all other locations around the core with the central Zn atom remaining in the system. Using the symmetry that prevails in the absence of the central Zn atom, we compute only the Zn/screw interaction for the site furthest from the added central Zn (which breaks the symmetry). The Zn/screw interaction energies are shown in figure 10. Unlike for the basal or prism edge dislocations, all of these interaction energies are negative. Furthermore, there is a large interaction energy of -0.27 eV for Zn in the central site in the core and of ~ -0.15 eV for several other sites near the center of the core. Such strong binding energies for all Zn solutes around the screw core suggest that the prism screw core could become metastable in the presence of random non-diffusing Zn solutes. Hence, random Zn solutes could facilitate nucleation of basal-prism kinks and cause the observed softening of prismatic slip at lower temperatures while possibly inhibiting basal/basal kink motion at

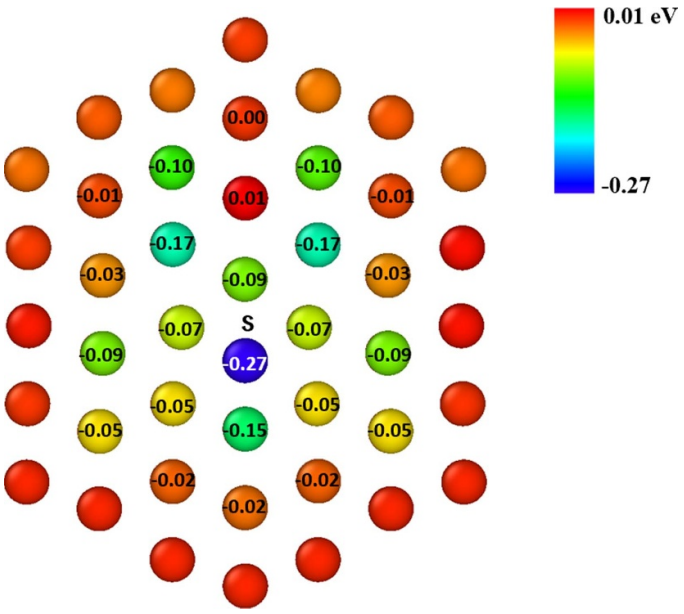

Figure 10. Zn/screw dislocation interaction energies for Zn solutes around the screw core, with some interaction energies shown explicitly. The S symbol indicates the center of the prism screw core.

higher temperatures. At higher temperatures, 'near-core' solute diffusion could stabilize the prism screw core even further and increase the stress required for screw motion. An analysis of the screw dislocation in Mg–Zn is well beyond the scope of the present study, but the results here provide an initial quantitative basis on which possible mechanisms can be studied in the future.

While the present work focuses on Mg–0.0045Zn, the general methods and concepts discussed here could be applied to other dilute alloy systems. Understanding the mechanism(s) of flow stress versus temperature and alloy composition, in the regime of where elevated deformation processing is performed, may be useful for tailoring alloy fabrication and performance.

Data availability statement

All data that support the findings of this study are included within the article (and any supplementary files).

Acknowledgments

This research was supported by the NCCR MARVEL, a National Centre of Competence in Research, funded by the Swiss National Science Foundation (Grant Numbers 205602 and 182892).

ORCID iD

M Rahbar Niazi https://orcid.org/0000-0003-4535-8164

References

[1] Ahmad R, Yin B, Wu Z and Curtin W A 2019 Designing high ductility in magnesium alloys *Acta Mater.* **172** 161–84
[2] Ahmad R, Wu Z and Curtin W A 2020 Analysis of double cross-slip of pyramidal I ⟨c+a⟩ screw dislocations and implications for ductility in Mg alloys *Acta Mater.* **183** 228–41
[3] Ahmad R, Wu Z, Groh S and Curtin W A 2018 Pyramidal II to basal transformation of ⟨c+a⟩ edge dislocations in Mg-Y alloys *Scr. Mater.* **155** 114–8
[4] Couret A and Caillard D 1985 An in situ study of prismatic glide in magnesium—I. The rate controlling mechanism *Acta Metall.* **33** 1447–54
[5] Couret A and Caillard D 1985 An in situ study of prismatic glide in magnesium—II. Microscopic activation parameters *Acta Metall.* **33** 1455–62
[6] Couret A, Caillard D, Püschl W and Schoeck G 1991 Prismatic glide in divalent h.c.p. metals *Phil. Mag.* A **63** 1045–57
[7] Liu X and Curtin W A 2024 Mechanism of thermally-activated prismatic slip in Mg *Acta Mater.* **262** 119402
[8] Ghafarollahi A and Curtin W A 2021 Theory of kink migration in dilute BCC alloys *Acta Mater.* **215** 117078
[9] Akhtar A and Teghtsoonian E 1969 Solid solution strengthening of magnesium single crystals—I alloying behaviour in basal slip *Acta Metall.* **17** 1339–49
[10] Tehranchi A, Yin B and Curtin W A 2018 Solute strengthening of basal slip in Mg alloys *Acta Mater.* **151** 56–66
[11] Wu Z, Ahmad R, Yin B, Sandlöbes S and Curtin W A 2018 Mechanistic origin and prediction of enhanced ductility in magnesium alloys *Science* **359** 447–52
[12] Wu Z and Curtin W A 2015 The origins of high hardening and low ductility in magnesium *Nature* **526** 62–67
[13] Miura S, Imagawa S, Toyoda T, Ohkubo K and Mohri T 2008 Effect of rare-earth elements Y and Dy on the deformation behavior of Mg alloy single crystals *Mater. Trans.* **49** 952–6
[14] Gao L, Chen R S and Han E H 2009 Effects of rare-earth elements Gd and Y on the solid solution strengthening of Mg alloys *J. Alloys Compd.* **481** 379–84
[15] Sandlöbes S, Pei Z, Friák M, Zhu L-F, Wang F, Zaefferer S, Raabe D and Neugebauer J 2014 Ductility improvement of Mg alloys by solid solution: *ab initio* modeling, synthesis and mechanical properties *Acta Mater.* **70** 92–104
[16] Rahbar Niazi M and Curtin W A 2023 Solute strengthening of prism edge dislocations in Mg alloys *Eur. J. Mech.* A **104** 105128
[17] Leyson G P M, Curtin W A, Hector L G and Woodward C F 2010 Quantitative prediction of solute strengthening in aluminium alloys *Nat. Mater.* **9** 750–5
[18] Varvenne C, Luque A and Curtin W A 2016 Theory of strengthening in fcc high entropy alloys *Acta Mater.* **118** 164–76
[19] Varvenne C, Leyson G P M, Ghazisaeidi M and Curtin W A 2017 Solute strengthening in random alloys *Acta Mater.* **124** 660–83
[20] Francesco M and Curtin W A 2020 Mechanistic origin of high strength in refractory BCC high entropy alloys up to 1900K *Acta Mater.* **182** 235–49
[21] Kresse G and Furthmüller J 1996 Efficient iterative schemes for ab initio total-energy calculations using a plane-wave basis set *Phys. Rev.* B **54** 11169–86
[22] Perdew J P, Burke K and Ernzerhof M 1996 Generalized gradient approximation made simple *Phys. Rev. Lett.* **77** 3865–8
[23] Blöchl P E 1994 Projector augmented-wave method *Phys. Rev.* B **50** 17953–79
[24] Methfessel M and Paxton A T 1989 High-precision sampling for Brillouin-zone integration in metals *Phys. Rev.* B **40** 3616–21
[25] Monkhorst H J and Pack J D 1976 Special points for Brillouin-zone integrations *Phys. Rev.* B **13** 5188–92
[26] Curtin W A, Olmsted D L and Hector L G 2006 A predictive mechanism for dynamic strain ageing in aluminium–magnesium alloys *Nat. Mater.* **5** 875–80
[27] Keralavarma S M, Bower A F and Curtin W A 2014 Quantum-to-continuum prediction of ductility loss in aluminium–magnesium alloys due to dynamic strain aging *Nat. Commun.* **5** 4604
[28] Leyson G P M, Hector L G and Curtin W A 2012 Solute strengthening from first principles and application to aluminum alloys *Acta Mater.* **60** 3873–84

[29] Soare M A and Curtin W A 2008 Single-mechanism rate theory for dynamic strain aging in fcc metals *Acta Mater.* **56** 4091–101
[30] Zhang F and Curtin W A 2008 Atomistically informed solute drag in Al–Mg *Modelling Simul. Mater. Sci. Eng.* **16** 055006
[31] James W and Barnett D M 1985 A re-examination of atmospheres and impurity drag on moving dislocations *Solute–Defect Interaction. Theory and Experiment* pp 136–42
[32] Liu X, Niazi M R, Liu T, Yin B and Curtin W A 2022 A low-temperature prismatic slip instability in Mg understood using machine learning potentials *Acta Mater.* **243** 118490